

CFD SIMULATION OF FLAME SPRAY PROCESS FOR SILICA NANOPOWDER SYNTHESIS FROM TETRAETHYLORTHOSILICATE (TEOS)

B. Wan,¹ Y. Ji,¹ H. Y. Sohn,¹ H. D. Jang,² and T. A. Ring³

1 Department of Metallurgical Engineering, University of Utah, Salt Lake City, Utah 84112

2. Nano-Materials Group, Korea Institute of Geoscience and Mineral Resources (KIGAM),
Daejeon, KOREA

3. Department of Chemical Engineering University of Utah, Salt Lake City, Utah 84112

Keywords: CFD; Simulation; Population Balance; Silica nanoparticles;
Tetraethylorthosilicate; Flame spray pyrolysis.

Abstract

The process of synthesizing silica nanopowder by the gas phase thermal oxidation of tetraethylorthosilicate (TEOS) in a diffusion flame reactor was simulated using a commercial computational fluid dynamic (CFD) code. The fuel combustion process and silica particle formation and growth in the flame are modeled. The temperature, velocity and particle size distribution (PSD) fields inside the reactor are computed. Chemical reaction rate and population balance model (PBM) were used to calculate the particle formation and growth and PSD.

Introduction

Silica (SiO₂) nanoparticles are used as additives in plastics and rubbers to improve mechanical properties of elastomers, and in liquid system to improve the suspension behavior. In these applications, the particle morphology, average size, size distribution, and phase composition are considered as the key characteristics of powders that must be controlled [1].

Flame aerosol process has been used to produce various nanoparticles such as ceramic, metal and composite powders because it provides good control of particle size and crystal structure. This method can also produce high-purity particles continuously without further treatments such as drying, calcinations and milling. The sizes of flame-made particles range from a few to several hundred nanometers, depending on process conditions [2,3].

In this work, a mathematical model of the flame reaction process for the synthesis of silicon compounds from tetraethylorthosilicate (TEOS) was created. The goal was to simulate experimental results obtained by Jang, described in various papers [4,5,6]. First a commercial CFD software package was adapted to the geometry and operating conditions of the flame reactor without including the particles to obtain the correct temperature and velocity fields of the hydrogen-oxygen flame. The silica particle nucleation and growth was then incorporated into the simulation through the use of the nucleation kinetics and particle growth model together with the population balance approach to keep track of the particle size distribution at any point within the reactor.

Modeling approach

In the experimental work by Jang [4, 5, 6], silica nanoparticles were synthesized by the gas phase thermal oxidation of tetraethylorthosilicate (TEOS) in a laminar diffusion flame reactor. A modified burner composed of five concentric tubes was developed by Jang and coworkers [4]. Silica nanoparticles ranged from 10 to 40 nm in average size were produced in their experiments.

The simulation of a flame reaction process involves the description of the fluid flow, heat and mass transfer processes, chemical reactions, and mixing of the gaseous components fuel, oxidant and precursor as well as the particle formation and growth. The model resulting from such an approach is most realistic and, more importantly, can be used to predict with greater confidence the results of the process operated under various other sets of conditions.

A commercial computer software Fluent was used as the main framework for the computation of the flame reaction process, by incorporating all the physical and chemical subprocesses described above

Computational mesh generation

We created 2-D system meshes for the reactor used in the experiment by Jang and coworkers [4]. Because of the axial symmetry of the reactor, only one half of the domain is needed for simulation. Each inlet opening was divided by a minimum of four cell widths. The entire domain was 300mm in length and 50mm in width. The number of cells in our successful runs for the hydrogen-oxygen flame simulation was 27027. This mesh design is shown in Fig. 1. This and the subsequent figures representing the reactor configuration show the vertical experimental reactor turned 90 degrees clockwise. Thus, the bottom side represents the vertical centerline of the reactor in Fig.1. (In some other figures the entire reactor is turned 90 degrees clockwise making the bottom the opposite wall.) The left side of the figure represents the bottom of the reactor with five concentric openings for raw material injection. The top of the figure represents the reactor wall and the right side represents the top of the reactor where the gas and particles leave the reactor. The meshes in the domain are not uniform. The nearer the centerline, the denser the meshes are. The nearer the inlet and outlet, the denser the meshes.

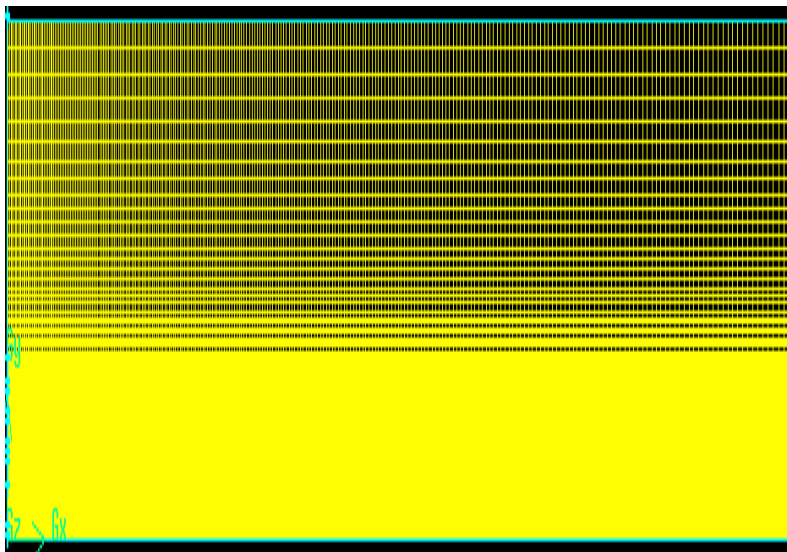


Figure 1. Overall mesh generation.

Figure 2 shows the details of the mesh design near the five raw material inlets of the modified diffusion flame burner composed of five concentric stainless tubes. Hydrogen (H₂) is used as a fuel while O₂ and air are used as oxidants. Argon (Ar) gas saturated with TEOS vapor was introduced to the central tube of the burner.

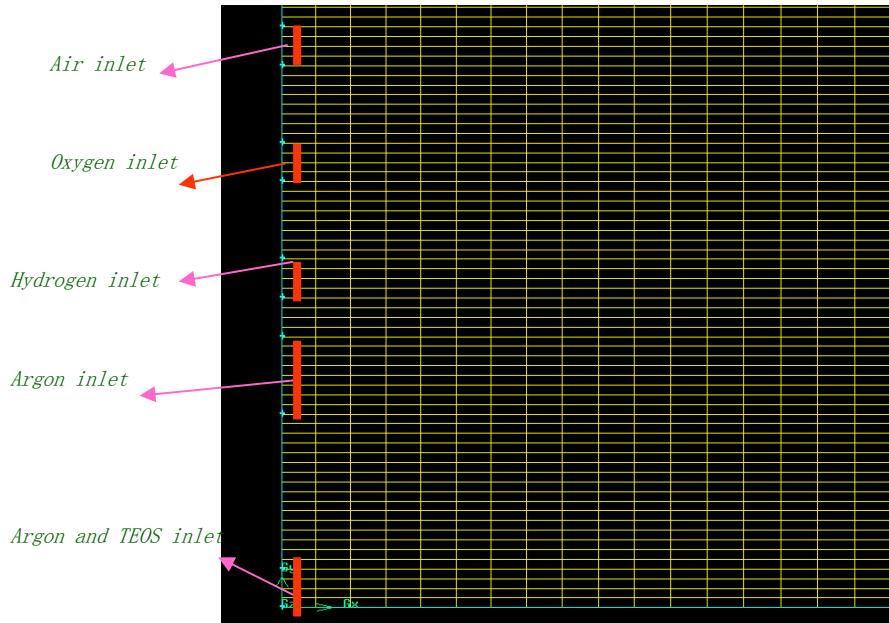


Figure 2. Details of the mesh design near the five raw material inlets

Computation Fluid Dynamics (CFD) process

Basic governing equations [6]. The following partial differential equations are solved to compute velocity, temperature, pressure and species concentration fields inside the reactor.

1) Momentum equations: Navier-Stokes equations (3D in Cartesian coordinates)

$$\rho \frac{\partial u}{\partial t} + \rho u \frac{\partial u}{\partial x} + \rho v \frac{\partial u}{\partial y} + \rho w \frac{\partial u}{\partial z} = -\frac{\partial \hat{p}}{\partial x} + \mu \left[\frac{\partial^2 u}{\partial x^2} + \frac{\partial^2 u}{\partial y^2} + \frac{\partial^2 u}{\partial z^2} \right] \quad (1)$$

$$\rho \frac{\partial v}{\partial t} + \rho u \frac{\partial v}{\partial x} + \rho v \frac{\partial v}{\partial y} + \rho w \frac{\partial v}{\partial z} = -\frac{\partial \hat{p}}{\partial y} + \mu \left[\frac{\partial^2 v}{\partial x^2} + \frac{\partial^2 v}{\partial y^2} + \frac{\partial^2 v}{\partial z^2} \right] \quad (2)$$

$$\rho \frac{\partial w}{\partial t} + \rho u \frac{\partial w}{\partial x} + \rho v \frac{\partial w}{\partial y} + \rho w \frac{\partial w}{\partial z} = -\frac{\partial \hat{p}}{\partial z} + \mu \left[\frac{\partial^2 w}{\partial x^2} + \frac{\partial^2 w}{\partial y^2} + \frac{\partial^2 w}{\partial z^2} \right] \quad (3)$$

2) Energy equations

$$\rho C_p \left(\frac{\partial T}{\partial t} + v_x \frac{\partial T}{\partial x} + v_y \frac{\partial T}{\partial y} + v_z \frac{\partial T}{\partial z} \right) = k \left[\frac{\partial^2 T}{\partial x^2} + \frac{\partial^2 T}{\partial y^2} + \frac{\partial^2 T}{\partial z^2} \right] + \mu \Phi_v + Source \quad (4)$$

where C_p is heat capacity, T is temperature, $Source$ can be chemical reaction or other energy production or consumption process, and Φ_v is the dissipation function. The term $\mu \Phi_v$ is usually negligible, except in systems with large velocity gradients.

3) Species transport equations:

$$\frac{\partial}{\partial t}(\rho Y_i) + \nabla \cdot (\rho \mathbf{v} Y_i) = -\nabla \cdot \mathbf{J}_i + R_i + S_i \quad (5)$$

where R_i is the net rate of production of species i by chemical reaction and S_i is the rate of creation by addition from the dispersed phase plus any user-defined sources. Y_i is mass fraction of each species. J_i is the diffusion flux of species i , which arises due to concentration gradients.

4) Continuity equation:

$$\frac{\partial \rho}{\partial t} + \frac{\partial(\rho u)}{\partial x} + \frac{\partial(\rho v)}{\partial y} + \frac{\partial(\rho w)}{\partial z} = 0 \quad (6)$$

5) Equation of state: $p = (\rho/MW) RT \quad (7)$

6) The population balance equation [7]:

$$\frac{\partial n}{\partial t} + \frac{\partial(Gn)}{\partial L} + n \frac{d(\log V)}{dt} = B - D - \sum_k \frac{Q_k n_k}{V} \quad (8)$$

where n is population density, B is birth rate, D is death rate, G is particle molecular growth rate.

Materials and operating and boundary conditions

The eight species considered in the simulation are H₂, O₂, H₂O, N₂, CO₂, Si(OC₂H₅)₄, (TEOS), SiO₂ and Ar. The total pressure is taken as 1 atm (101.3 kPa). We specify the inlet mass fraction for each species in our simulation. For example, we set mass fraction of TEOS as 0.6% (based on 2.5x10⁻⁴ mol/l) in the Argon and TEOS inlet. In some runs, we have varied the mass fraction of TEOS to calculate its effect. At the walls, Fluent applies a zero-gradient (zero-flux) boundary condition for all species (standard wall function) and temperature is kept at 298 K.

We start with the initial values for temperature at 2000 K, O₂ mass fraction of 0.23, H₂ mass fraction of 0.1 and Si(OC₂H₅)₄ mass fraction of 10⁻⁸. The residues for continuity, x-velocity, y-velocity and energy are set at 10⁻⁶ as the conversion criteria, the residues of six moments (moments 0~5) are set at 10⁻⁴ and the others at 10⁻³.

Combustion and chemical reaction

The species transport and finite-rate chemistry modeling, which is one of the five combustion modeling approached in Fluent, was chosen for this work. The reaction rates that appear as source terms are computed by combined finite-rate/eddy-dissipation model.

For laminar finite-rate model: The effects of turbulent fluctuations are ignored, and the rate constants are presented by Arrhenius expressions.

$$k_f = A_r T^{\beta_r} \exp(-E_r/RT) \quad (9)$$

where A_r is pre-exponential factor (consistent units); β_r is temperature exponent (dimensionless); E_r is activation energy for the reaction (J/kmol); R is universal gas constant (J/kmol-K).

For eddy-dissipation model, reaction rates are assumed to be controlled by the turbulence, and thus extensive Arrhenius chemical kinetic calculations can be avoided. The model is computationally cheap, but for realistic results, only one or two step heat-release mechanisms should be used.

The net rate of production of species i due to reaction, $R_{i,r}$, is given by the smaller (i.e., limiting value) of the two expressions below:

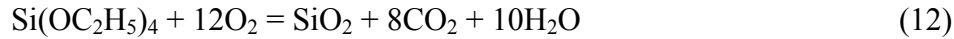
$$R_{i,r} = v'_{ir} M_{\omega,i} AB \rho \frac{\epsilon(10) \sum_P Y_P}{k \sum_j v''_{j,r} M_{\omega,j}}$$

$$R_{i,r} = v'_{ir} M_{\omega,i} A \rho \frac{\epsilon(11)}{k} \min\left(\frac{Y_R}{v'_{R,r} M_{\omega,R}}\right)$$

where Y_P is the mass fraction of any product species, P ; Y_R is the mass fraction of a particular reactant, R ; A is an empirical constant equal to 4.0; B is an empirical constant equal to 0.5.

In this work, the combined finite-rate/eddy-dissipation model is used, where both the Arrhenius and eddy-dissipation reaction rates are calculated. The net reaction rate is taken as the minimum of these two rates.

The computation started by forming the flame based on the reaction of H_2 and O_2 . For this purpose, the TEOS and Ar inlet stream was replaced by pure Ar. When the result is converged, we added the oxidation reaction of TEOS:



We mixed 0.6 wt% of TEOS in an argon carrier gas in the TEOS input stream through the innermost feed tube. Because of the small amount of TEOS added, the results for the profiles of temperature, mass density, and concentrations of hydrogen, oxygen, water vapor, nitrogen and argon remain essentially unchanged. However, this further gives us confidence that we can add other gas-phase reactions and the numerical simulation still remains stable. The concentrations of the products, silica and carbon dioxide, of the oxidation of TEOS were obtained and shown below.

Particle formation and growth.

Different nucleation rate and growth rate models were tested in our calculation. Finally the following models were chosen based on the compromise of accuracy and easy implementation.

The linear growth rate of a particle under the control of mass transfer is given by

$$G_c = 4 * V_{mol} * D_{AB} * 1.013 * 10^5 / 8.314 / T * (1-1/S) * m_0 / m_1 * Y_{SiO_2}, \quad (13)$$

where V_{mol} is mole volume of the silica particle (m^3/mol); D_{AB} is diffusion coefficient; S is the degree of supersaturation (equals to P_{SiO_2} / P_{SiO_2} at saturation); m_0 is the Zeroth moment ($1/m^3$) of the particle size distribution; m_1 is the first moment (m/m^3); (thus, m_1/m_0 represents the number-averaged particle size); Y_{SiO_2} is mole fraction of SiO_2 in the gas phase.

G_m is defined as the growth rate under the control of chemical kinetics:

$$G_m = K_g * (S-1)^{N_g}, \quad (14)$$

where K_g represents the rate constant and the exponent N_g was assumed to be 1. The total growth rate G_t then can be calculated by:

$$G_t = (G_c * G_m) / (G_c + G_m) \quad (16)$$

In terms of the particle growth rate, the rate of increase of the solid mass per unit volume of the system is given by:

$$\text{Source} = (\pi / 2) m_2 \cdot G \cdot \rho, \quad (15)$$

where ρ is solid density (kg/m^3) and m_2 is second moment of the particle size distribution (m^2/m^3), which represents the total surface area of particles per unit volume of the reactor.

Assuming power-law kinetics for the nucleation rate, then nucleation rate can be calculated by:

$$J = K_n \cdot (S-1)^{N_n}, \quad (16)$$

where J is Nucleation rate; K_n is the rate constant; and the exponent N_n equals 1.

The results for the size distribution characteristics of the silica particles produced by the oxidation of TEOS in a flame reaction process are expressed in terms of the appropriate moments of the size distribution. The i^{th} moment m_i is defined by

$$m_i = \int_0^{\infty} L^i n(L) dL \quad (17)$$

where L is particle size, $n(L)$ is the particle number density function. The final particle size distribution are obtained by solving population balance equation using SMOM and QMOM method [7, 8, 9].

Results and discussion

Temperature and velocity profile results and discussion

Figure 3 shows the converged result, which indicates that the computed temperature field is very realistic in terms of the magnitude and distribution of temperature. It is highest where the main fuel hydrogen comes in contact with oxygen and decreased in the axial and radial directions, enveloped within a region reasonably shaped like a flame.

The distribution of the velocity magnitude, shown in Fig. 4, is reasonable in both axial and radial directions. This converged result gave us confidence that the simulation was correct as far as the velocity as a function of position was concerned.

The contours of the stream function (the iso-stream function lines), shown in Fig. 5, represent the paths of the fluid elements. Further, the magnitude of the stream function indicates the flow rate between two adjacent lines. It is seen that the radial expansion of the gas flow is simulated correctly and the magnitude of the flow rate is reasonable. In addition, the presence of a recirculating zone is indicated accurately. This converged result adds to our confidence for the computation of the velocity field under the experimental conditions to be simulated.

After some 20,000 iterations, the solution was converged (shown as Figure 6). The residual is under 10^{-6} . It takes more than 10 hours of computation on a computer with Pentium 4, 3G Hz processor and 1 G Hz memory. All the pictures shown in this paper are converged. (Different case required different iterations and computation time.)

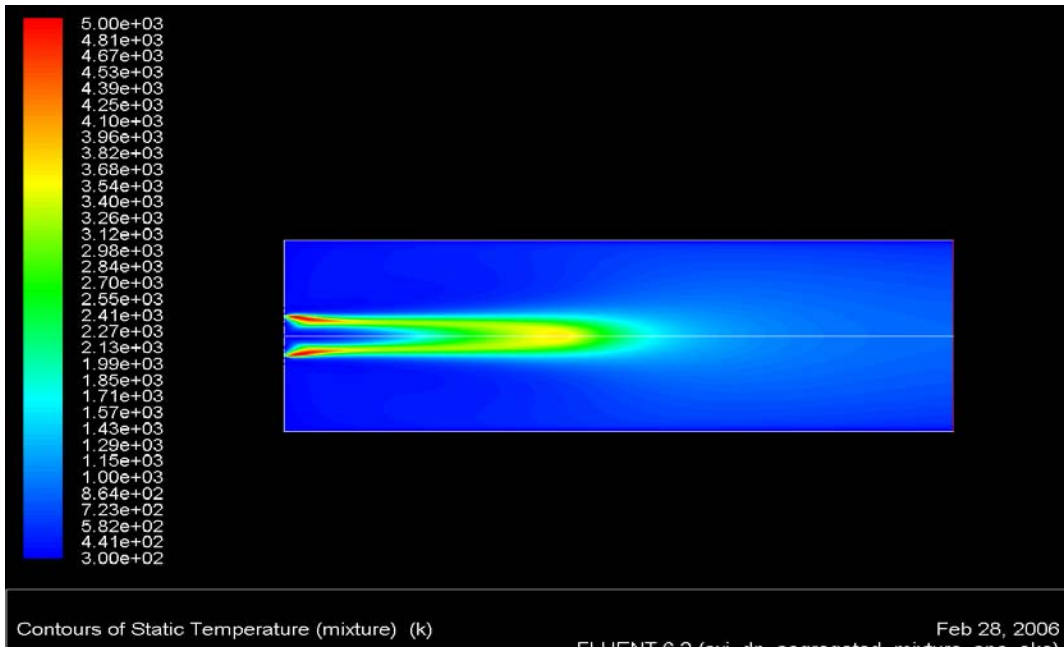


Figure 3. Contours of temperature (K)

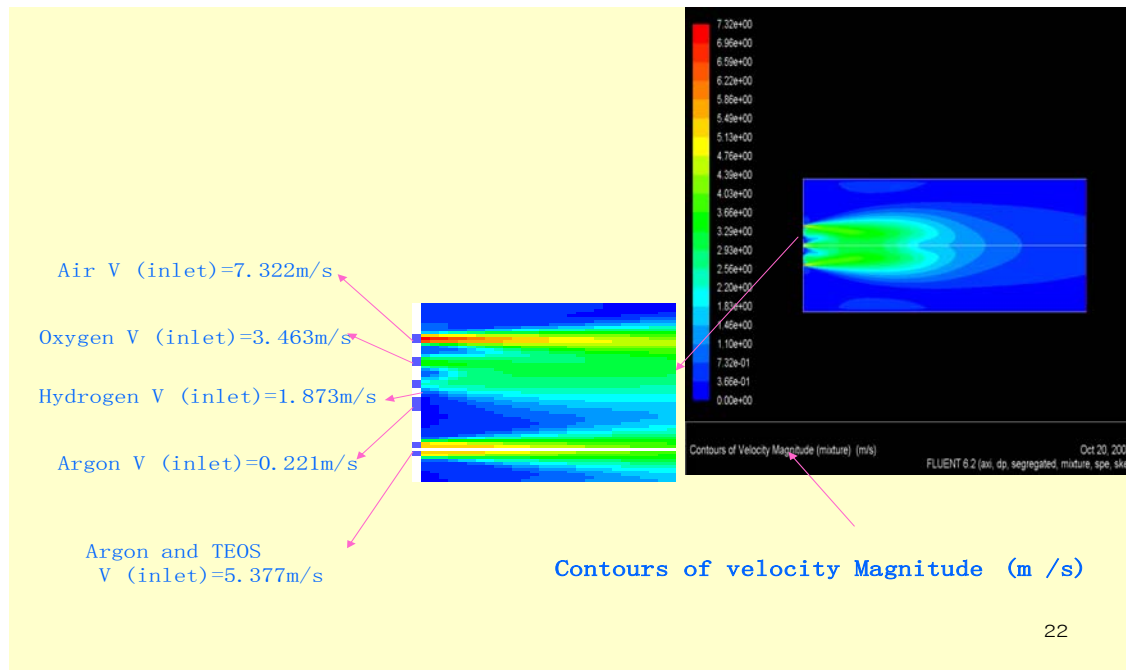


Figure 4. Contours of velocity magnitude

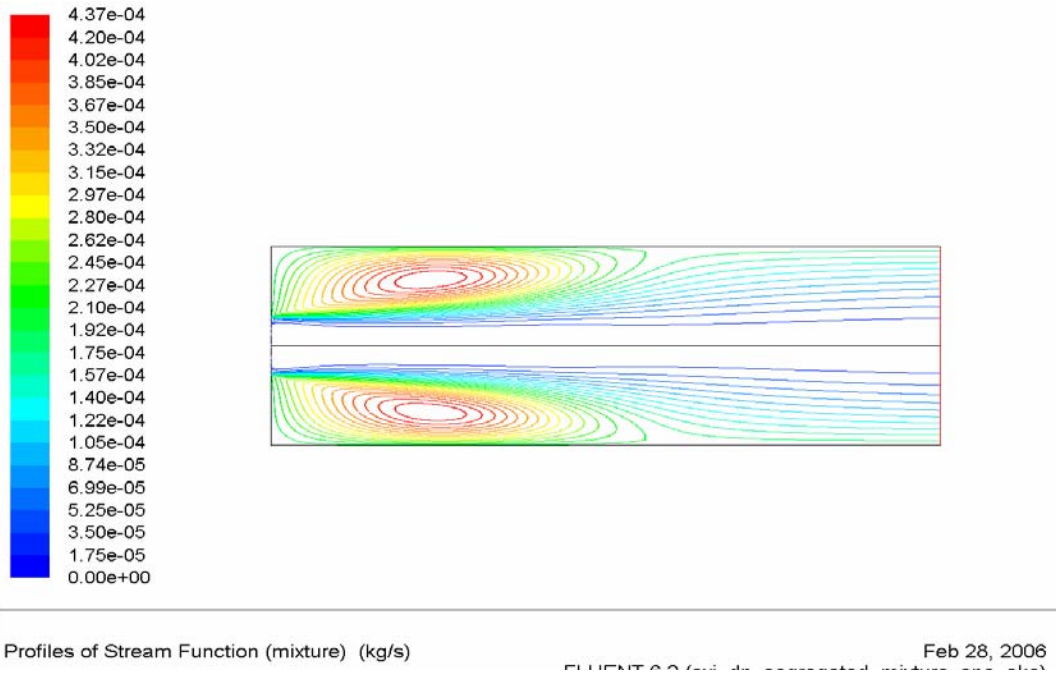


Figure 5. Contours of stream function

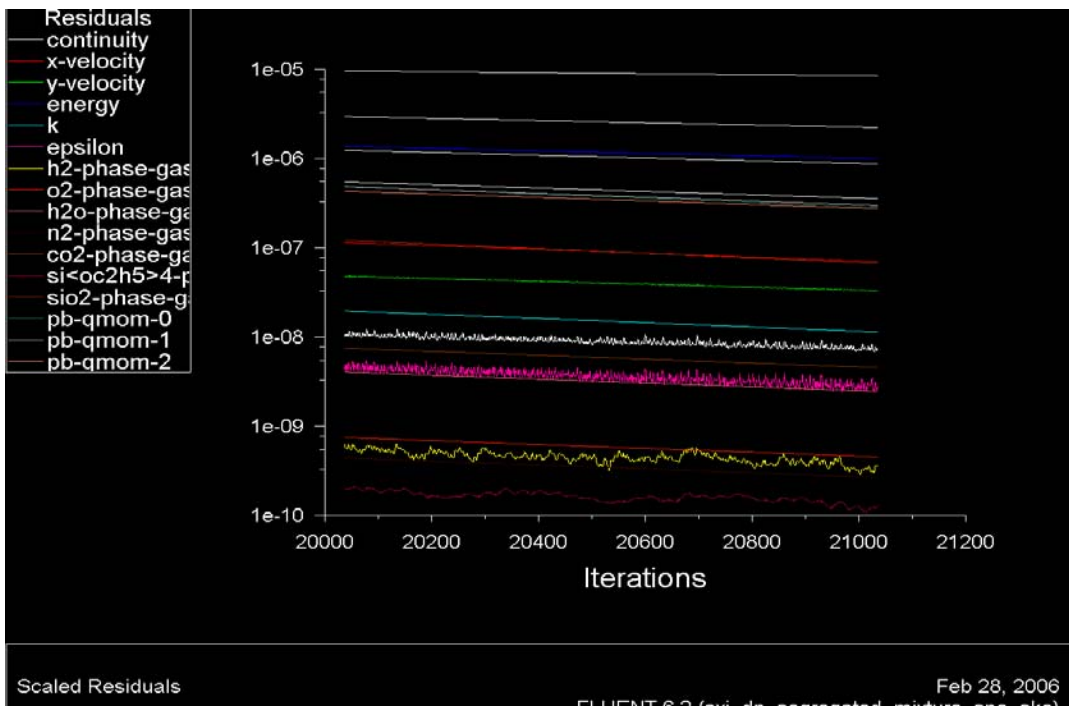


Figure 6. Scaled residuals for all variables

Particle distribution profile and discussion

Figures 7~9 are the typical examples of the particle size distribution computed with different combination of Kn and Kg values. The particle sizes match the result of experiment well. These results are obtained by the quadrature method of moments (QMOM)

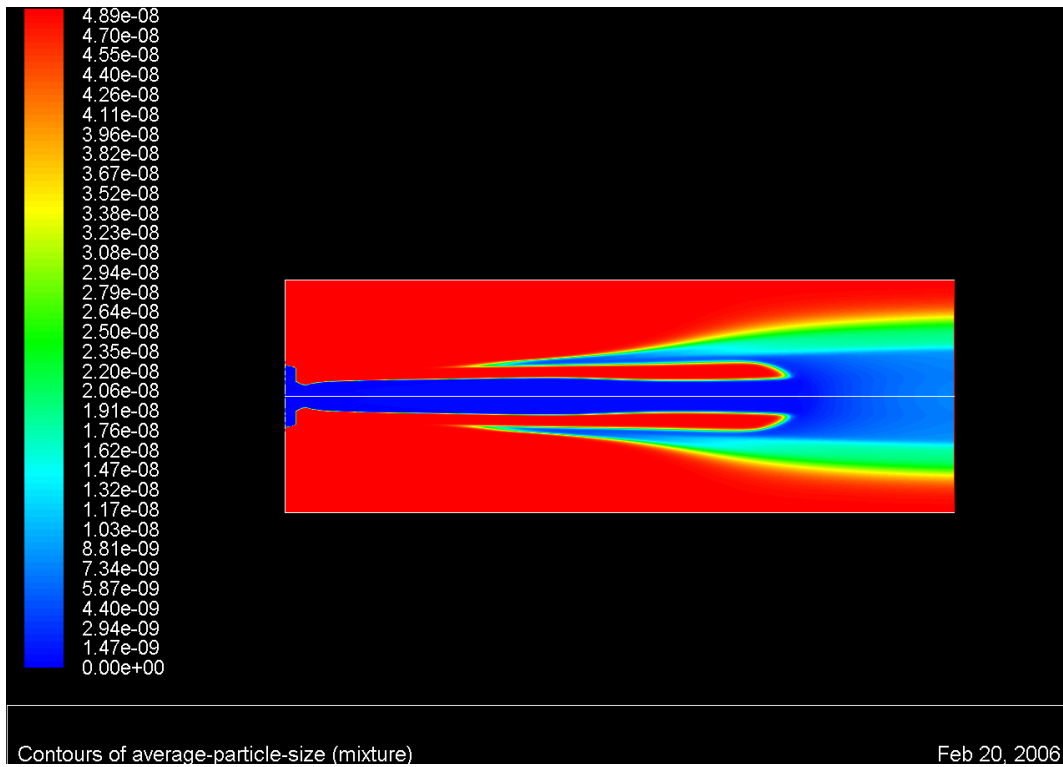


Figure 7. Contours of volume average particle size (m) ($Kn=10$, $Kg=10^{-24}$)

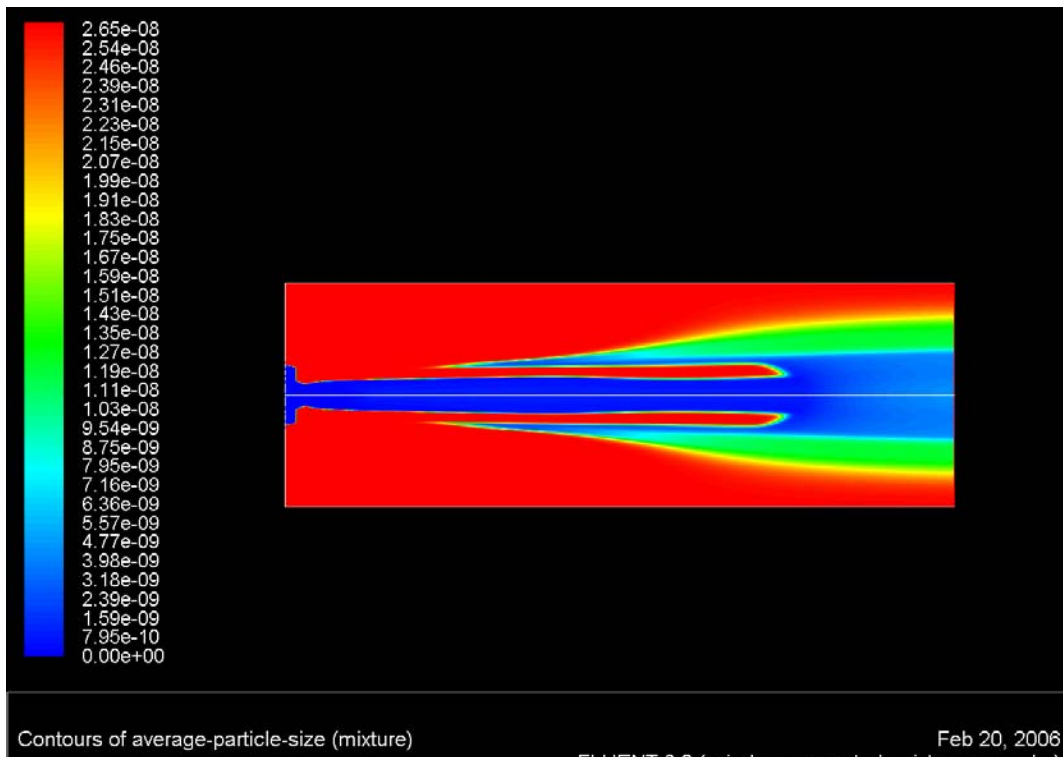


Figure 8. contours of volume average particle size (m) ($Kn=10^2$, $Kg=10^{-24}$)

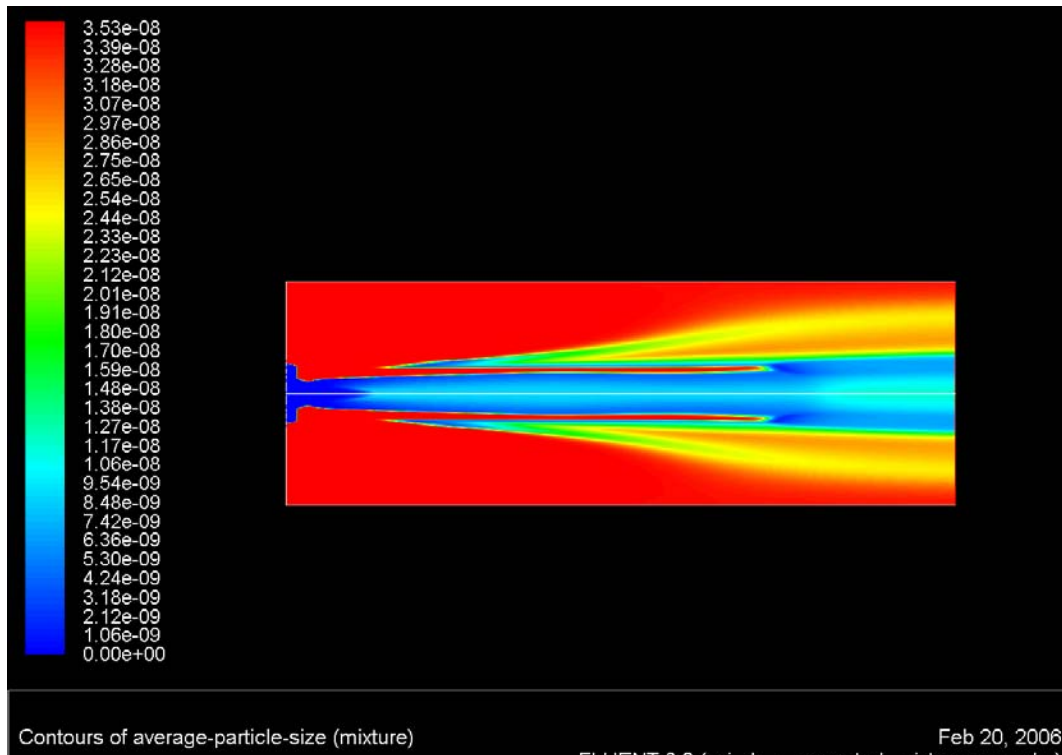


Figure 9. contours of volume average particle size (m) ($Kn=10^2$, $Kg=10^{-23}$)

These figures show the average particle size inside the reactor at any point. It is obtained by dividing the fourth moment of the particle size distribution function by the third moment. From this, we see that the average particle size is small close to the centerline and larger close to the wall. The reason is because the particle stays longer near the wall.

Table 1 summarizes the calculated particle size distribution parameters from the converged results computation with various combinations of the nucleation rate constant Kn and the particle growth rate constant Kg in Eqs. (16) and (14), respectively, which yield average particle size in and near the experimentally observed range of 10 – 40 nm [4]. Because there are no independently measured data on these parameters for the system being simulated, we took the approach to perform a parametric study to investigate the effect of these parameters on the particle size distribution.

From this table, it is seen that a 10-fold increase in the nucleation rate constant Kn for the same growth rate constant results in the decrease of the particle size by approximately half. This agrees with the fact that when the nucleation rate increases by 10 times, approximately 10 times more particles form and the average particle volume reduces to one-tenth. Thus, the particle size decreases to the cubic root of one tenth, i.e $1/2.154$ which is about half the original size.

When and if more detailed experimental data for become available, additional model verification and validation can be performed, especially in terms of obtaining reliable values of the rate constants and with respect to the effects of process conditions as well as the spread in particle size distribution.

Table I Converged results with various combinations of nucleation and growth rate constants.
(TEOS concentration is 0.06%, based on 2.5×10^{-4} mol/l [4])

Kn	Kg	Average particle size (m ⁴ /m ³) (m)	C.V.= [m ⁵ *m ³ /(m ⁴) ² -1] ^{1/2}
1×10^{-2}	1×10^{-26}	2.518×10^{-8}	0.4397
1×10^{-2}	1×10^{-25}	1.085×10^{-7}	0.482
1×10^{-1}	1×10^{-26}	2.335×10^{-8}	0.4467
1×10^{-1}	1×10^{-25}	6.166×10^{-8}	0.4915
1	1×10^{-26}	1.752×10^{-8}	0.4659
1	1×10^{-25}	3.377×10^{-8}	0.4997
1	1×10^{-24}	5.504×10^{-8}	0.5853
10	1×10^{-25}	1.828×10^{-8}	0.5132
10	1×10^{-24}	3.021×10^{-8}	0.6157
10	1×10^{-23}	4.751×10^{-8}	0.513
1×10^2	1×10^{-25}	9.974×10^{-9}	0.5448
1×10^2	1×10^{-24}	1.640×10^{-8}	0.6241
1×10^2	1×10^{-23}	2.548×10^{-8}	0.4153
1×10^3	1×10^{-26}	3.377×10^{-9}	0.4997
1×10^3	1×10^{-25}	5.504×10^{-9}	0.5853
1×10^3	1×10^{-24}	8.870×10^{-9}	0.5953
1×10^3	1×10^{-22}	2.520×10^{-8}	0.3727
1×10^4	1×10^{-25}	3.020×10^{-9}	0.6131
1×10^4	1×10^{-24}	4.750×10^{-9}	0.513
1×10^4	1×10^{-23}	7.716×10^{-9}	0.3567

Concluding remarks

A two-dimensional CFD simulation was implemented to model the flame spray process for silica nano-powder synthesis from TEOS. Different operating conditions were tested. The combinations of assumed values of Kn and Kg that yield results that are consistent with experimental data have been identified. This work proved that by using CFD, more details of combustion and particle distribution and forming inside reactor can be obtained. This simulation work can be improved further by using finer mesh, and using a more accurate nucleation and growth model.

Acknowledgments

The authors wish to express their thanks to Professor Philip J. Smith, Dr. Jennifer Spinti, and Mr. Eric Mortenson of the Department of Chemical Engineering, University of Utah for their contribution with respect to CFD modeling during the early stage of this work. Financial support for this research from the Korea Institute of Geoscience and Mineral Resources (KIGAM) is gratefully acknowledged.

Y. Ji thanks the College of Mines and Earth Sciences, University of Utah for a Cooper-Hansen Fellowship that she received during the course of this work.

-
- [1] R.W. Siegel, Annual Review of Material Science, 21 (1991) 559.
- [2] T.T. Kodas, M.J. Hampden-Smith, Aerosol Processing of Material, p66 Wiley-VCH, New York (1999)
- [3] S.K. Friedlander, Smoke, Dust, and Haze: Fundamental of Aerosol Dynamics, p331 Oxford, New York (2000).
- [4] H. D. Jang, "Experimental Study of Synthesis of Silica Nanoparticles by a bench-scale Diffusion Flame Reactor", Powder Technology, 119 (2001) 102-108
- [5] H. D. Jang, "Generation of silica nanoparticles from tetraethylorthosilicate (TEOS) vapor in a diffusion flame," Aerosol Sci. Technol. 30, 477-488 (1999).
- [6] H. D. Jang, H. Chang, Y. Suh, and K. Okuyama, "Synthesis of SiO₂ Nanoparticles from Sprayed Droplets of Tetraethylorthosilicate by the Flame Spray Pyrolysis," personal communication, 2005.
- [7] A. D. Randolph and M. A. Larson, Theory of Particulate Processes, 2nd ed.; Academic Press: New York, 1988.
- [8] B. Wan, Computational Fluid Dynamics Simulation of Crystallization Process – Verification of Fluent's Population Balance Modeling, PhD thesis, University of Utah, August 2005
- [9] D. L Marchisio; A.. A. Barresi .; R. O Fox, AIChE Journal 2001, 47(3).